mathematics

MDPI

Article

Adaptive Backstepping Terminal Sliding Mode Control of Nonlinear System Using Fuzzy Neural Structure

Xiaoyu Gong [1], Wen Fu [2], Xingao Bian [2] and Juntao Fei [1,2,*]

[1] College of IoT Engineering, Jiangsu Key Laboratory of Power Transmission and Distribution Equipment Technology, Hohai University, Changzhou 213022, China
[2] College of Mechanical and Electrical Engineering, Hohai University, Changzhou 213022, China
* Correspondence: jtfei@hhu.edu.cn; Tel.: +86-519-8519-2023

Abstract: An adaptive backstepping terminal sliding mode control (ABTSMC) method based on a multiple−layer fuzzy neural network is proposed for a class of nonlinear systems with parameter variations and external disturbances in this study. The proposed neural network is utilized to estimate the nonlinear function to handle the unknown uncertainties of the system and reduce the switching term gain. It has a strong learning ability and high approximation accuracy due to the combination of a fuzzy neural network and recurrent neural network. The neural network parameters can be adaptively adjusted to optimal values through the adaptive laws derived from the Lyapunov theorem. To stabilize the control signal, the additional parameter adaptive law derived by the adaptive projection algorithm is used to estimate the control coefficient. The terminal sliding mode control (TSMC) is introduced on the basis of backstepping control, which can ensure that the tracking error converges in finite time. The simulation example is carried out on the DC–DC buck converter model to verify the effectiveness and superiority of the proposed control method. The contrasting results show that the ABTSMC−DHLRNN possesses higher steady−state accuracy and faster transient response.

Keywords: multiple−layer fuzzy neural network; recurrent neural network; adaptive projection algorithm; adaptive backstepping terminal sliding mode control

MSC: 68T07; 93C40

Citation: Gong, X.; Fu, W.; Bian, X.; Fei, J. Adaptive Backstepping Terminal Sliding Mode Control of Nonlinear System Using Fuzzy Neural Structure. *Mathematics* **2023**, *11*, 1094. https://doi.org/10.3390/math11051094

Academic Editor: Sundarapandian Vaidyanathan

Received: 27 January 2023
Revised: 14 February 2023
Accepted: 20 February 2023
Published: 22 February 2023

1. Introduction

It is well known that most systems existing in a variety of scenarios are nonlinear systems with a strict feedback form. The control purpose is to ensure that the state signals of the system follow the reference signals. As the loading conditions and system parameters are highly uncertain, it will lead to an undesirable impact on system regulation accuracy. Therefore, it is necessary to design a stable and adaptive controller for a nonlinear system with the presence of external disturbances and parameter variations.

It can be seen from early research that the PID controller has been widely concerned due to its simple principle and application. In [1], a PID controller was designed to suppress current harmonics for a permanent−magnet synchronous motor (PMSM). Irfan et al. [2] designed double PID controllers per axis for a stable flight of Vertical Take−Off and Landing drones. In order to handle the rapid variation in unknown disturbances, a dynamic parameter tuning method for variable PID controllers was proposed in [3]. Moreover, Meza et al. [4] presented a fuzzy self−tuning method to select PID gains according to the actual state of the model. However, the PID controller is a linear control strategy, which seldom ensures large−signal stability and robustness. Hence, more advanced control strategies are proposed to handle the instability problem. In [5], a proportional−integral−fuzzy controller based on an iterative feedback tuning algorithm was designed to control a class

of servo systems. In recent research, some nonlinear control methods have been widely used, including sliding mode control (SMC) [6] and backstepping control [7].

The main feature of backstepping control is that it designs virtual control laws for each subsystem through a step−by−step recursive process, which can reduce the complexity of the control design. Cai et al. [8] proposed a robust adaptive control strategy based on the backstepping technique for nonlinear systems with unknown parameters, and Lin et al. [9] designed an adaptive backstepping speed control system for a PMSM. However, when system uncertainty and disturbances are involved, it is difficult for conventional backstepping control to achieve high performance.

Due to the design of the switching term, SMC is another attractive choice for application in the nonlinear system, which has the property of robustness to disturbances. In [10], a second−order SMC algorithm was presented to solve motion control problems of robot manipulators. In [11], a super−twisting algorithm was introduced into SMC, which can effectively weaken the chattering phenomenon of the control input. Here, the backstepping sliding mode control (BSMC) was proposed, which combines both characteristics of backstepping control and SMC. It has also been developed in various scenarios such as multimachine power systems [12], hypersonic vehicles [13], unmanned aerial vehicles [14], and DC microgrids [15].

However, SMC can only guarantee that the tracking error asymptotically converges to zero. With respect to this problem, the terminal SMC (TSMC) has attracted more attention, which can ensure the finite−time convergence of the tracking error, thus improving the dynamic property of the system [16]. Yao et al. [17] developed a robust adaptive nonsingular TSMC (NTSMC) in the position and speed control of an automatic train operation system. Wang et al. [18] adopted continuous TSMC to realize the trajectory tracking of flexible−joint robots, and Xu et al. [19] introduced a novel nonsingular fast TSMC−reaching law to shorten the response time of the controlled model.

Although SMC can alleviate the adverse effects of system uncertainty and external disturbances, it often causes the high−frequency chattering problem due to a large switching term gain. Moreover, the computation of the control signal depends on exact parameter information of the system, which is not available in actual application. Some scholars have developed adaptive sliding mode control (ASMC) [20,21]. In [20], an ASMC was presented for parameter estimation in a boost converter through the use of state observers. In addition, Xu and Yao [22] utilized the bounds on the parameters to construct an adaptive projection algorithm, which ensures that the estimates belong to a known bounded region. However, when dealing with fast time−varying parameters, control action through ASMC alone is not reliable. This disadvantage is overcome by employing a neural network feedforward control method of estimating the nonlinear function.

The neural network (NN) has a strong learning ability, which is widely applied in the control of unknown systems. In [23], a novel NN−based controller was presented to obtain the reference tracking control of a nonlinear position servo system, and the neural network was trained by a Deep Q−Learning algorithm.

The radial basis function neural network (RBFNN), as a common network structure, is obtained in nonlinear systems with unknown nonlinearities [24]. Moreover, a novel self−organizing RBFNN was reported in [25], where the structure of the RBFNN can be regulated according to the system behavior. Considering the low approximation capability of the RBFNN, and that it takes a long time to adjust weights, this is not a favorable choice.

The fuzzy neural network (FNN) possesses the learning ability of neural networks and inference capability of fuzzy systems in handling unknown information, which have been developed rapidly for dynamic modeling and advanced controllers design [26–29]. Lin et al. [30] proposed a Takagi–Sugeno–Kang fuzzy neural network to estimate the lumped uncertainty. The recurrent neural network (RNN) uses the cyclic connection technique, and the neuron feedback loop is utilized to transmit previous output signals, which means that the network considers the previous dynamic information to improve the connection dependency in layers. Therefore, the RNN has the ability to handle time−varying

inputs and external disturbances. A self−organizing RNN with a general nonlinear form for predicting system behaviors is proposed in [31]. However, it is difficult for the RNN with a single hidden layer to maintain high approximation accuracy, which will also increase the calculation computation due to the necessity of a large number of neurons. Thus, the RNN with a double−loop structure was proposed [32,33]. In [33], this network structure was designed for identification and prediction of the motion control system. However, conventional single−layer neural networks may need to train numerous neurons, which will cause the increase in computational complexity and the excessive consumption of high memory. Therefore, a multiple−layer neural network (MLNN) structure has been widely concerned, which can provide fewer neurons training and higher approximation accuracy. Lee et al. [34] designed a multiple−spatiotemporal−scale recurrent neural network for action recognition. It was reported in [35] that a convolutional multiple−layer recurrent neural network can be used for both homogeneous and heterogeneous images. In [36], a multilayer perceptron neural network was developed as an exploratory test oracle. Some fuzzy neural controllers were investigated to enhance the approximation capability of neural networks for dynamic systems [37–43].

Based on the merits of FNN, RNN, and MLNN, this paper designs a multiple−layer fuzzy neural network structure, i.e., double−hidden−layer recurrent neural network (DHLRNN), which introduces double hidden layers and double loop feedbacks, suppressing the adverse effects of external disturbances and dealing with the uncertainty of the nonlinear systems.

Based on the above research, an adaptive backstepping terminal sliding mode control based on the DHLRNN is proposed in this paper. The DHLRNN and parameter adaptive law derived from the projection algorithm are utilized to estimate the unknown function and control coefficient of the universal nonlinear system, respectively, and the estimated value is then transferred to the controller for effective feedforward compensation. Moreover, the proposed SMC method combines the features of backstepping control and TSMC; under the framework of such a control strategy, the system can obtain faster transient responses. The main contributions of the proposed control method compared with existing works are summarized as follows:

(1) The proposed DHLRNN inherits the fuzzy inference ability of the FNN, and includes the self−regulation ability of the RNN, which can be used to estimate more complex unknown functions. Therefore, the DHLRNN can counteract and compensate system uncertainties to improve the tracking accuracy of the control system. As an improvement of the single−hidden−layer neural network, the DHLRNN contains two−layer activation functions for feature extraction. It can process complex data and avoid serious calculation complexity by reducing the number of neurons.

(2) This paper utilizes Lyapunov stability theory to derive the adaptive laws of the DHLRNN. The parameters including base width, center vector, and feedback weights can be trained online. The neural network output can be continuously updated according to the system parameter variations. This means that the proposed neural network will reach the optimal value after a short learning and adjustment. The proposed controller can obtain dynamic regulation instead of relying on exact mathematical models. The adaptive law of the control coefficient derived from Lyapunov theory adopts an expression form of a projection algorithm, which ensures that the estimated value changes in a known bounded region. Whether faced with disturbances or not, the control coefficient remains bounded all the time, and the stability of control signal can be guaranteed.

(3) The design of backstepping TSMC not only reduces the complexity of control design, but also makes the state tracking error converge in finite time. The use of the switching term can also counteract the adverse effects of external disturbances and the lumped approximation error of the neural network to improve the steady−state performance and anti−disturbance performance of the system.

The rest of this paper is organized as follows. Section 2 introduces the state equation of nonlinear systems and the problem statement is presented. In Section 3, the design of the proposed control method is given, including the neural network definition and stability proof. The simulation study is shown in Section 4. Finally, Section 5 concludes this paper.

2. System Description and Problem Statement

Consider the following a class of a SISO partially unknown nonlinear system

$$\begin{cases} \dot{x}_1 = x_2 \\ \dot{x}_2 = x_3 \\ \vdots \\ \dot{x}_{n-1} = x_n \\ \dot{x}_n = f(X) + bu + d(t) \end{cases} \tag{1}$$

where $X = [x_1 \quad x_2 \quad \cdots \quad x_n]^T$ is the state vector, and $f(X)$ and b are a nonlinear function and control coefficient, respectively. u denotes the control signal and $d(t)$ denotes the external disturbance.

Due to the parameter variations and measurement limitations, the system parameters are difficult to obtain accurately; there exists $f(X) = f_0(X) + \Delta f(X)$, where $f_0(X)$ is the nominal part of the nonlinear function and $\Delta f(X)$ is the unknown uncertainty. $\Delta f(X)$ is considered upper−bounded. The control coefficient b is considered bounded.

The main control objective is to design an appropriate control signal u so that the state signal X can accurately track the reference trajectory X_r, i.e.,

$$\lim_{t\to\infty} |X - X_r| = \lim_{t\to\infty} |E| = 0 \tag{2}$$

where $X_r = [x_r, \dot{x}_r, \cdots, x_r^{(n-1)}]^T$ and $E = [e, \dot{e}, \cdots, e^{(n-1)}]^T$ is the error vector.

The BTSMC method is presented for the control problem; $f(X)$ and b are assumed to be known. Moreover, the terminal function $p(t)$ is introduced into the backstepping control to ensure finite−time convergence, and the sliding surface is built by the backstepping control variables.

Remark 1. *Consider that the terminal function $p(t)$ is a continuous differentiable function with n order. In order to obtain global robustness, the condition of $e^{(i)}(0) = p^{(i)}(0)$, $i = 0, 1, \cdots, n-1$ is established. Moreover, for the set time $T > 0$, when $t \geq T$, $p(t) = 0$, $\dot{p}(t) = 0, \cdots, p^{(n)}(t) = 0$ should be satisfied to obtain finite−time convergence of the tracking error. Therefore, the terminal function is defined as*

$$p(t) = \begin{cases} \sum_{k=0}^{n} \frac{1}{k!} e(0)^{(k)} t^k + \sum_{j=0}^{n} \sum_{l=0}^{n} [\frac{a_{jl}}{T^{j-l+n+1}} e(0)^{(l)}]\, t^{j+n+1}, & if\ 0 \leq t \leq T \\ 0, & if\ t > T \end{cases} \tag{3}$$

The terminal function coefficients a_{jl} can be calculated by solving the equations $p(T) = 0$, $\dot{p}(T) = 0$, $\cdots$, $p^{(n)}(T) = 0$.

The detailed design process is described as the following steps

Step 1 Design of the virtual control term α_1

(i) Define the tracking error $z_1 = x_1 - x_r - p$;

(ii) Design the virtual control term $\alpha_1 = -k_1 z_1$, where $k_1 > 0$.

Step 2 Design of the virtual control term α_2

(i) Define the tracking error $z_2 = x_2 - \dot{x}_r - \dot{p} - \alpha_1$;

(ii) Design the virtual control term $\alpha_2 = -k_2 z_2 - z_1 + \dot{\alpha}_1$, where $k_2 > 0$;

(iii) Take the derivative of z_1: $\dot{z}_1 = -k_1 z_1 + z_2$.

Step i Design of the virtual control term α_i

(i) Define the tracking error $z_i = x_i - x_r^{(i-1)} - p^{(i-1)} - \alpha_{i-1}$;
(ii) Design the virtual control term $\alpha_i = -k_i z_i - z_{i-1} + \dot{\alpha}_{i-1}$, where $k_i > 0$;
(iii) Take the derivative of z_{i-1}: $\dot{z}_{i-1} = z_i - k_{i-1} z_{i-1} - z_{i-2}$.

Step n Design of the control law

(i) Define the tracking error $z_n = x_n - x_r^{(n-1)} - p^{(n-1)} - \alpha_{n-1}$;
(ii) Design the following terminal sliding surface $s = cz_{n-1} + z_n$, where $c > 0$;
(iii) Take the derivative of z_{n-1}: $\dot{z}_{n-1} = z_n - k_{n-1} z_{n-1} - z_{n-2}$;
(iv) Take the derivative of z_n: $\dot{z}_n = f(X) + bu + d(t) - x_r^{(n)} - p^{(n)} - \dot{\alpha}_{n-1}$;
(v) Design an equivalent control law u_{eq}: $u_{eq} = \frac{1}{b}[-c(-k_{n-1} z_{n-1} - z_{n-2} + z_n) - z_{n-1} - f(X) + x_r^{(n)} + p^{(n)} + \dot{\alpha}_{n-1}]$;
(vi) Design a switching control law u_{sw}: $u_{sw} = \frac{1}{b}[-\rho s - \lambda \text{sign}(s)]$, where $\rho > 0$, $\lambda > D$, and $sign(\cdot)$ denotes a sign function;
(vii) Design the ideal control law u: $u = u_{eq} + u_{sw}$.

Theorem 1. *For SISO nonlinear system (1), when all parameter information of the system is known and the external disturbance $d(t)$ is bounded, if the terminal sliding surface is chosen as*

$$s = cz_{n-1} + z_n \tag{4}$$

and the ideal controller using a switching term is designed as

$$\begin{aligned} u &= u_{eq} + u_{sw} \\ &= \frac{1}{b}[-c(-k_{n-1} z_{n-1} - z_{n-2} + z_n) - z_{n-1} - f(X) + x_r^{(n)} + p^{(n)} + \dot{\alpha}_{n-1} - \rho s - \lambda \text{sign}(s)] \end{aligned} \tag{5}$$

all signals of the closed−loop system will asymptotically converge to zero.

Proof. The Lyapunov function is selected as

$$V = \frac{1}{2}\sum_{i=1}^{n-1} z_i^2 + \frac{1}{2}s^2 \tag{6}$$

Taking the first derivative of (6) and combining the relationship between z_i and sliding surface s, it can be obtained that

$$\begin{aligned} \dot{V} &= \sum_{i=1}^{n-1} z_i \dot{z}_i + s\dot{s} = -\sum_{i=1}^{n-1} k_i z_i^2 + z_{n-1} z_n + s\dot{s} \\ &= -\sum_{i=1}^{n-1} k_i z_i^2 + z_{n-1} z_n + s[c(-k_{n-1} z_{n-1} - z_{n-2} + z_n) \\ &\quad + f(X) + bu + d(t) - x_r^{(n)} - p^{(n)} - \dot{\alpha}_{n-1}] \end{aligned} \tag{7}$$

Substituting control input (5) into (7) obtains

$$\begin{aligned} \dot{V} &= -\sum_{i=1}^{n-1} k_i z_i^2 + z_{n-1}(s - cz_{n-1}) + s(-z_{n-1} - \rho s - \lambda \text{sign}(s) + d(t)) \\ &= -\sum_{i=1}^{n-1} k_i z_i^2 - cz_{n-1}^2 - \rho s^2 - \lambda |s| + sd(t) \\ &\le -\sum_{i=1}^{n-1} k_i z_i^2 - cz_{n-1}^2 - \rho s^2 - \lambda |s| + D|s| \end{aligned} \tag{8}$$

Assume $|d(t)| \leq D$, where D is an unknown positive constant. When the condition $\lambda > D$ is satisfied, the following inequality holds:

$$\begin{aligned} \dot{V} &\leq -\sum_{i=1}^{n-1} k_i z_i^2 - c z_{n-1}^2 - \rho s^2 - (\lambda - D)|s| \\ &\leq -\sum_{i=1}^{n-1} k_i z_i^2 - c z_{n-1}^2 - \rho s^2 \end{aligned} \tag{9}$$

Therefore, inequality (9) satisfies $\dot{V} \leq 0$. According to the LaSalle invariance principle, the convergence of backstepping control variables and the sliding surface can be guaranteed, i.e., when $t \to \infty$, then $z_i = 0$ $(i = 1, 2, \cdots n)$, $s = 0$. Moreover, the tracking error E will converge to zero in finite time under the constraint of terminal function $p(t)$. The detailed proof is shown in Remark 5. □

Remark 2. *When the Lyapunov function and system control law are selected, then the condition of* $\lim_{s \to 0} s\dot{s} \leq 0$ *is derived, and it can be concluded that* $\lim_{s \to 0^+} \dot{s} \leq 0$ *and* $\lim_{s \to 0^-} \dot{s} \geq 0$. *This means that as long as there are state signals close to switching surface* $s(x) = 0$, *they will be attracted and fluctuate around the switching surface. Therefore, according to the designed sliding mode trajectory, the state signals can reach the specified region*.

3. Design of Adaptive Backstepping Terminal Sliding Mode Controller Using Dhlrnn

Although the ideal control signal designed in (5) can guarantee the convergence of all states and signals of the nonlinear system (1), an accurate mathematical model is difficult to obtain because of environmental fluctuations and disturbances. Control actions through SMC alone result in a large switching term gain, which will cause system chattering and damage the steady−state performance of the system. In order to observe the real−time information of the model, this section utilizes the DHLRNN and parameter adaptive laws to estimate the nonlinear function $f(X)$ and control coefficient b, respectively, and the estimated value is introduced into the controller for effective feedforward compensation to improve control accuracy.

3.1. Structure of DHLRNN

The specific structure of the proposed neural network is shown in Figure 1, which comprises the input layer (layer 1), the first hidden layer (layer 2), the second layer (layer 3), and the output layer (layer 4).

The proposed DHLRNN is a multi−layer network structure and possesses self−learning ability, which combines the advantages of the FNN and RNN. It can be used to estimate complex nonlinear functions, which provides an effective solution to the unknown uncertainty problem of the system.

The detailed signal transmission and the basic function in each layer of the DHLRNN are introduced as follows

Layer 1 (Input Layer): The main function of this layer is to pass the input variables to the next layer. Due to the design of external feedback, the output value exY at the previous time is connected to the input layer by the feedback weight $W_{roi} (i = 1, 2, \cdots, m)$, thus providing the optimal input for the subsequent processing. For every node in the input layer, the ith node output is calculated as follows:

$$\theta_i = x_i \cdot W_{roi} \cdot exY, \ (i = 1, 2, \cdots, m) \tag{10}$$

where x_i denotes the input of the ith node, $X = [x_1, x_2, \cdots, x_m]^T$ is the input vector in this layer, and $\theta = [\theta_1, \theta_2, \cdots, \theta_m]^T$ is the output vector. The external feedback weight matrix of the input layer is described as

$$W_{ro} = [W_{ro1}, W_{ro2}, \cdots, W_{rom}]^T \tag{11}$$

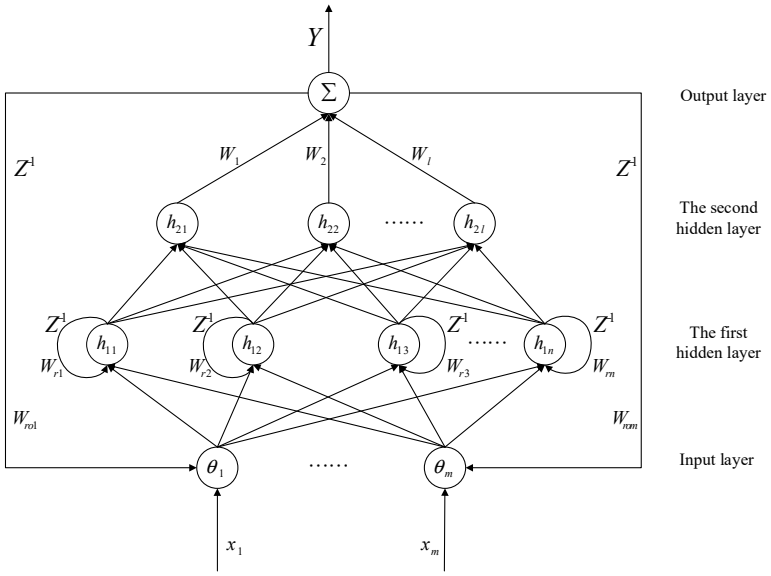

Figure 1. Structure of the proposed neural network.

Layer 2 (The First hidden layer): This layer adopts a Gaussian function as an activation function to realize fuzzification operation with the aim to expand the dimension of the input variables. The signal is mapped from the low−dimensional space to the high−dimensional space. The internal feedback loop is realized and the dynamic recursion leads to better mapping, which improves the neuron activation intensity. The output form of the jth node is expressed as

$$\begin{aligned} \phi_{1j} &= e^{-net_{1j}},\ (j = 1, 2, \cdots, n) \\ net_{1j} &= \sum_{i=1}^{m} \frac{(\theta_i \cdot W_{rj} \cdot L\phi_{1j} - c_{1j})^2}{b_{1j}^2} \end{aligned} \tag{12}$$

where b_{1j} and c_{1j} are the center vector and the base width of the jth activation function, respectively. $L\phi_{1j}$ represents the previous output of the jth node, which will be fed back to the current node through the feedback weight W_{rj}. The output vector of the first hidden layer is $\Phi_1 = [\phi_{11}, \phi_{12}, \cdots, \phi_{1n}]^T$. The center vector matrix, base width matrix, and feedback weight matrix of the first hidden layer are, respectively, described as

$$B_1 = [b_{11}, b_{12}, \cdots, b_{1n}]^T \tag{13}$$

$$C_1 = [c_{11}, c_{12}, \cdots, c_{1n}]^T \tag{14}$$

$$W_r = [W_{r1}, W_{r2}, \cdots, W_{rn}]^T \tag{15}$$

Layer 3 (The second hidden layer): This layer also utilizes Gaussian function for nonlinear mapping, which is similar to the function of the first hidden layer. The signals are mapped from the first hidden layer space to the higher−dimensional space, and the features of the input vector are further extracted. The kth node output of the second hidden layer is expressed as

$$\begin{aligned} \phi_{2k} &= e^{-net_{2k}},\ (k = 1, 2, \cdots, l) \\ net_{2k} &= \sum_{j=1}^{n} \frac{(\phi_{1j} - c_{2k})^2}{b_{2k}^2} \end{aligned} \tag{16}$$

where b_{2k} and c_{2k} denote the center vector and the base width, respectively. $\Phi_2 = [\phi_{21}, \phi_{22}, \cdots, \phi_{2l}]^T$ is the output vector of the second hidden layer. The center vector matrix and base width matrix of the second hidden layer are, respectively, described as

$$B_2 = [b_{21}, b_{22}, \cdots, b_{2l}]^T \tag{17}$$

$$C_2 = [c_{21}, c_{22}, \cdots, c_{2l}]^T \tag{18}$$

Layer 4 (Output layer): This layer will calculate the overall output of the network and serve as the feedback signal of the input layer. The single output node is connected with each neuron of the second hidden layer by the weight $W_k (k = 1, 2, \cdots, l)$, which is labeled with the symbol Σ. The output of the DHLRNN is the weighted sum of the Gaussian function calculated by the second hidden layer, expressed as

$$Y = W^T \Phi_2 = \sum_{k=1}^{l} W_k \phi_{2k} \tag{19}$$

where the weight matrix of the output layer is described as

$$W = [W_1, W_2, \cdots, W_l]^T \tag{20}$$

Based on the number of nodes m, n, l in each layer, the proposed DHLRNN structure is defined as $m - n - l - 1$, which can be selected carefully according to the specific system.

3.2. Approximation Error of DHLRNN

The DHLRNN is used to estimate the nonlinear function in the ideal controller (5), and there exists B_1^*, C_1^*, W_r^*, B_2^*, C_2^*, W_{ro}^*, and W^*, satisfying the following expression

$$f(X) = {W^*}^T \Phi_2^*(B_1^*, C_1^*, W_r^*, B_2^*, C_2^*, W_{ro}^*) + \varepsilon \tag{21}$$

where ε is the reconstruction error between the optimal value and actual value, bounded as: $\varepsilon \leq \varepsilon_N$, and ε_N is a positive constant.

The optimal parameters of the DHLRNN are obtained from the following equation

$$\begin{aligned} &\left(B_1^*, C_1^*, W_r^*, B_2^*, C_2^*, W_{ro}^*, W^*\right) \\ &= \underset{(B_1, C_1, W_r, B_2, C_2, W_{ro}, W)}{\operatorname{argmin}} [\sup \| f - f^* \|] \end{aligned} \tag{22}$$

The estimated value of $f(X)$ is the real output of the neural network, expressed as

$$\hat{f}(X) = \hat{W}^T \hat{\Phi}_2(\hat{B}_1, \hat{C}_1, \hat{W}_r, \hat{B}_2, \hat{C}_2, \hat{W}_{ro}) \tag{23}$$

where $\hat{W}, \hat{B}_1, \hat{C}_1, \hat{W}_r, \hat{B}_2, \hat{C}_2, \hat{W}_{ro}$ are the estimated values of the neural network parameters.

Therefore, the approximation error between the estimated value and actual value is defined as

$$\begin{aligned} f - \hat{f} &= {W^*}^T \Phi_2^* - \hat{W}^T \hat{\Phi}_2 + \varepsilon \\ &= {W^*}^T \left(\hat{\Phi}_2 + \widetilde{\Phi}_2\right) - \hat{W}^T \hat{\Phi}_2 + \varepsilon \\ &= {W^*}^T \hat{\Phi}_2 + {W^*}^T \widetilde{\Phi}_2 - \hat{W}^T \hat{\Phi}_2 + \varepsilon \\ &= \left(\hat{W}^T + \widetilde{W}^T\right) \hat{\Phi}_2 + \left(\hat{W}^T + \widetilde{W}^T\right) \widetilde{\Phi}_2 - \hat{W}^T \hat{\Phi}_2 + \varepsilon \\ &= \widetilde{W}^T \hat{\Phi}_2 + \hat{W}^T \widetilde{\Phi}_2 + \varepsilon_0 \end{aligned} \tag{24}$$

where $\varepsilon_0 = \widetilde{W}^T \widetilde{\Phi}_2 + \varepsilon$ denotes the total approximation error and $\widetilde{W} = W^* - \hat{W}$ is the weight error.

In order to convert nonlinear $f(X)$ into a partially linear form, the Taylor expansion linearization technique is used in this paper. The Taylor expansion of the optimal output

vector Φ_2^* of the second hidden layer at $B_1^* = \hat{B}_1$, $C_1^* = \hat{C}_1$, $W_r^* = \hat{W}_r$, $B_2^* = \hat{B}_2$, $C_2^* = \hat{C}_2$, and $W_{ro}^* = \hat{W}_{ro}$ can be calculated as follows

$$\begin{aligned}\Phi_2^*(B_1^*, C_1^*, W_r^*, B_2^*, C_2^*, W_{ro}^*) &= \hat{\Phi}_2(\hat{B}_1, \hat{C}_1, \hat{W}_r, \hat{B}_2, \hat{C}_2, \hat{W}_{ro}) \\ &+ \frac{\partial \Phi_2}{\partial B_1^*}\Big|_{B_1^*=\hat{B}_1}(B_1^* - \hat{B}_1) + \frac{\partial \Phi_2}{\partial C_1^*}\Big|_{C_1^*=\hat{C}_1}(C_1^* - \hat{C}_1) \\ &+ \frac{\partial \Phi_2}{\partial W_r^*}\Big|_{W_r^*=\hat{W}_r}(W_r^* - \hat{W}_r) + \frac{\partial \Phi_2}{\partial B_2^*}\Big|_{B_2^*=\hat{B}_2}(B_2^* - \hat{B}_2) \\ &+ \frac{\partial \Phi_2}{\partial C_2^*}\Big|_{C_2^*=\hat{C}_2}(C_2^* - \hat{C}_2) + \frac{\partial \Phi_2}{\partial W_{ro}^*}\Big|_{W_{ro}^*=\hat{W}_{ro}}(W_{ro}^* - \hat{W}_{ro}) + O_h\end{aligned} \tag{25}$$

$$\begin{aligned}&\widetilde{\Phi}_2(\widetilde{B}_1, \widetilde{C}_1, \widetilde{W}_r, \widetilde{B}_2, \widetilde{C}_2, \widetilde{W}_{ro}) = \Phi_{2B_1} \cdot \widetilde{B}_1 + \Phi_{2C_1} \cdot \widetilde{C}_1 \\ &+\Phi_{2W_r} \cdot \widetilde{W}_r + \Phi_{2B_2} \cdot \widetilde{B}_2 + \Phi_{2C_2} \cdot \widetilde{C}_2 + \Phi_{2W_{ro}} \cdot \widetilde{W}_{ro} + O_h\end{aligned} \tag{26}$$

where O_h is a high−order term of expansion; Φ_{2B_1}, Φ_{2C_1}, Φ_{2W_r}, Φ_{2B_2}, Φ_{2C_2}, and $\Phi_{2W_{ro}}$ are first−order partial derivatives of Φ_2 to B_1^*, C_1^*, W_r^*, B_2^*, C_2^*, and W_{ro}^*, respectively. These partial derivatives conform to the arrangement of the Jacobian matrix, which can be expressed, respectively, as the following forms:

$$\Phi_{2B_1} = \begin{bmatrix} \frac{\partial \phi_{21}}{\partial b_{11}} & \cdots & \frac{\partial \phi_{21}}{\partial b_{1n}} \\ \vdots & \ddots & \vdots \\ \frac{\partial \phi_{2l}}{\partial b_{11}} & \cdots & \frac{\partial \phi_{2l}}{\partial b_{1n}} \end{bmatrix}_{l \times n} \tag{27}$$

$$\Phi_{2C_1} = \begin{bmatrix} \frac{\partial \phi_{21}}{\partial c_{11}} & \cdots & \frac{\partial \phi_{21}}{\partial c_{1n}} \\ \vdots & \ddots & \vdots \\ \frac{\partial \phi_{2l}}{\partial c_{11}} & \cdots & \frac{\partial \phi_{2l}}{\partial c_{1n}} \end{bmatrix}_{l \times n} \tag{28}$$

$$\Phi_{2W_r} = \begin{bmatrix} \frac{\partial \phi_{21}}{\partial W_{r1}} & \cdots & \frac{\partial \phi_{21}}{\partial W_{rn}} \\ \vdots & \ddots & \vdots \\ \frac{\partial \phi_{2l}}{\partial W_{r1}} & \cdots & \frac{\partial \phi_{2l}}{\partial W_{rn}} \end{bmatrix}_{l \times n} \tag{29}$$

$$\Phi_{2B_2} = \begin{bmatrix} \frac{\partial \phi_{21}}{\partial b_{21}} & \cdots & \frac{\partial \phi_{21}}{\partial b_{2l}} \\ \vdots & \ddots & \vdots \\ \frac{\partial \phi_{2l}}{\partial b_{21}} & \cdots & \frac{\partial \phi_{2l}}{\partial b_{2l}} \end{bmatrix}_{l \times l} \tag{30}$$

$$\Phi_{2C_2} = \begin{bmatrix} \frac{\partial \phi_{21}}{\partial c_{21}} & \cdots & \frac{\partial \phi_{21}}{\partial c_{2l}} \\ \vdots & \ddots & \vdots \\ \frac{\partial \phi_{2l}}{\partial c_{21}} & \cdots & \frac{\partial \phi_{2l}}{\partial c_{2l}} \end{bmatrix}_{l \times l} \tag{31}$$

$$\Phi_{2W_{ro}} = \begin{bmatrix} \frac{\partial \phi_{21}}{\partial W_{ro1}} & \cdots & \frac{\partial \phi_{21}}{\partial W_{rom}} \\ \vdots & \ddots & \vdots \\ \frac{\partial \phi_{2l}}{\partial W_{ro1}} & \cdots & \frac{\partial \phi_{2l}}{\partial W_{rom}} \end{bmatrix}_{l \times m} \tag{32}$$

Substituting partial derivatives (27)–(32) into (24), the approximation error can be further expressed as

$$\begin{aligned}f(X) - \hat{f}(X) &= \widetilde{W}^T\hat{\Phi}_2 + \hat{W}^T\widetilde{\Phi}_2 + \varepsilon_0 \\ &= \widetilde{W}^T\hat{\Phi}_2 + \hat{W}^T\Phi_{2C_1}\widetilde{C}_1 + \hat{W}^T\Phi_{2C_2}\widetilde{C}_2 \\ &+\hat{W}^T\Phi_{2B_1}\widetilde{B}_1 + \hat{W}^T\Phi_{2B_2}\widetilde{B}_2 + \hat{W}^T\Phi_{2W_r}\widetilde{W}_r \\ &+\hat{W}^T\Phi_{2W_{ro}}\widetilde{W}_{ro} + \Delta_0\end{aligned} \tag{33}$$

where $\Delta_0 = \hat{W}^T O_h + \varepsilon_o$ denotes the lumped high−order approximation error.

Assumption 1. *Due to the approximation capability of the DHLRNN, the lumped high−order approximation error of the DHLRNN, i.e.,* Δ_o*, is much smaller than the function being estimated, i.e.,* $f(X)$*.* Δ_o *is bounded and satisfies* $|\Delta_o| \leq \overline{\Delta}_d$*, where* $\overline{\Delta}_d$ *is a positive constant.*

3.3. Stability Analysis

The block diagram of ABTSMC based on the proposed DHLRNN is shown in Figure 2. The neural network parameters are updated online through the adaptive laws, so the output of the neural network can adaptively adjust to the optimal value. The flowchart of the learning algorithm of the proposed controller is provided in Figure 3, which comprises the detailed algorithm description. Furthermore, an additional parameter adaptive law is adopted to estimate the control coefficient b for guaranteeing the stability of the control law u, and the corresponding estimated value is denoted as $\hat{b}$.

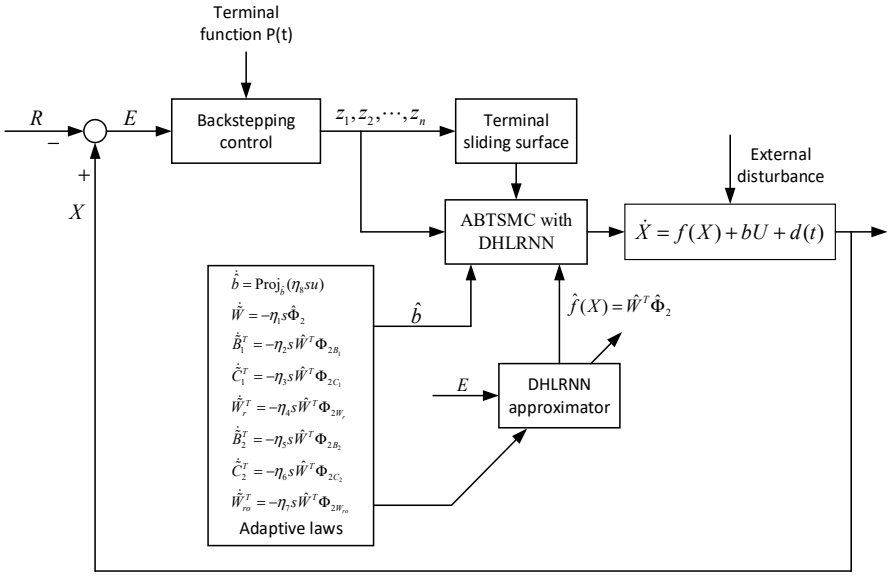

Figure 2. Block diagram of the ABTSMC using DHLRNN.

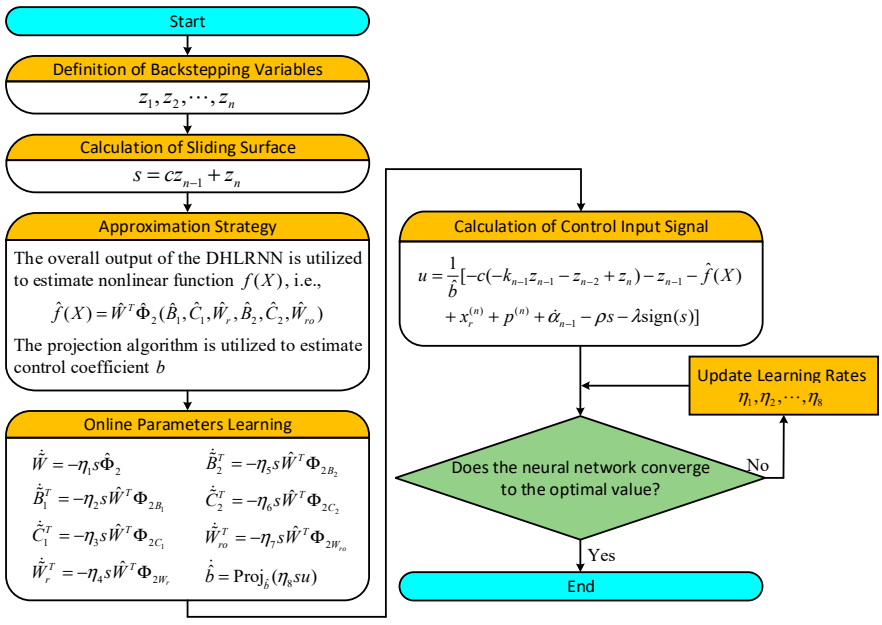

Figure 3. The flowchart of learning algorithm of the proposed controller.

As the DHLRNN and parameter adaptive law introduce the estimated information of the system into the controller, the control system can maintain robustness in rejecting uncertainties and disturbances. The proposed control method no longer depends on the accurate mathematical model, which is more suitable for an actual nonlinear system.

Based on the designed feedforward compensation technology, the new control law is designed as

$$\begin{aligned} u = \; & \tfrac{1}{\hat{b}}[-c(-k_{n-1}z_{n-1} - z_{n-2} + z_n) - z_{n-1} - \hat{f}(X) \\ & + x_r^{(n)} + p^{(n)} + \dot{\alpha}_{n-1} - \rho s - \lambda \mathrm{sign}(s)] \end{aligned} \tag{34}$$

Theorem 2. *For SISO nonlinear system (1), when the external disturbance $d(t)$ and control coefficient b are both bounded, if the control law of system is chosen as (34), then it guarantees that all signals of the closed−loop system will asymptotically converge to zero.*

Proof. The new Lyapunov function is selected as

$$\begin{aligned} V = \; & \tfrac{1}{2}\sum_{i=1}^{n-1} z_i^2 + \tfrac{1}{2}s^2 + \tfrac{1}{2\eta_1}\widetilde{W}^T\widetilde{W} + \tfrac{1}{2\eta_2}\widetilde{B}_1^T\widetilde{B}_1 + \tfrac{1}{2\eta_3}\widetilde{C}_1^T\widetilde{C}_1 \\ & + \tfrac{1}{2\eta_4}\widetilde{W}_r^T\widetilde{W}_r + \tfrac{1}{2\eta_5}\widetilde{B}_2^T\widetilde{B}_2 + \tfrac{1}{2\eta_6}\widetilde{C}_2^T\widetilde{C}_2 + \tfrac{1}{2\eta_7}\widetilde{W}_{ro}^T\widetilde{W}_{ro} + \tfrac{1}{2\eta_8}\widetilde{b}^2 \end{aligned} \tag{35}$$

where $\widetilde{b} = b - \hat{b}$ is the approximation error of the control coefficient; η_1, η_2, η_3, η_4, η_5, η_6, η_7, and η_8 are the learning rates parameters. □

Remark 3. *According to the main control objective, in order to ensure that the state signal can track the reference trajectory, the convergence of backstepping intermediate variables, the sliding surface, and the estimated term must be guaranteed. Specially, the seven adaptive parameters of the DHLRNN including center vectors, base widths, output weight, and feedback weight should converge to the optimal value so that the neural network can approximate the real−time variation in the nonlinear function accurately. Motivated by the abovementioned ideas, the Lyapunov function should contain three parts: backstepping intermediate variables $z_i (i = 1, 2, \cdots, n-1)$, sliding surface s, and estimation error of all parameters. Moreover, according to the Lyapunov stability theory, we must guarantee that the designed Lyapunov function is positive definite and its derivative is semi−negative definite. Therefore, the new Lyapunov function is constructed as provided in (35).*

Taking the first derivative of the Lyapunov function (35), and then substituting the relationship between $z_i (i = 1, 2, \cdots, n)$ and sliding surface s into the derivative, yields

$$\begin{aligned} \dot{V} &= \sum_{i=1}^{n-1} z_i\dot{z}_i + s\dot{s} + H = -\sum_{i=1}^{n-1} k_i z_i^2 + z_{n-1}z_n + s\dot{s} + H \\ &= -\sum_{i=1}^{n-1} k_i z_i^2 + z_{n-1}z_n + s[c(-k_{n-1}z_{n-1} - z_{n-2} + z_n) \\ &\quad + f(X) + bu + d(t) - x_r^{(n)} - p^{(n)} - \dot{\alpha}_{n-1}] + H \end{aligned} \tag{36}$$

where

$$\begin{aligned} H = \; & \tfrac{1}{\eta_1}\widetilde{W}^T\dot{\widetilde{W}} + \tfrac{1}{\eta_2}\dot{\widetilde{B}}_1^T\widetilde{B}_1 + \tfrac{1}{\eta_3}\dot{\widetilde{C}}_1^T\widetilde{C}_1 + \tfrac{1}{\eta_4}\dot{\widetilde{W}}_r^T\widetilde{W}_r \\ & + \tfrac{1}{\eta_5}\dot{\widetilde{B}}_2^T\widetilde{B}_2 + \tfrac{1}{\eta_6}\dot{\widetilde{C}}_2^T\widetilde{C}_2 + \tfrac{1}{\eta_7}\dot{\widetilde{W}}_{ro}^T\widetilde{W}_{ro} - \tfrac{1}{\eta_8}\widetilde{b}\dot{\hat{b}} \end{aligned} \tag{37}$$

Substituting the proposed control law (34) into (37) obtains

$$\begin{aligned} \dot{V} = \; & -\sum_{i=1}^{n-1} k_i z_i^2 + z_{n-1}(s - cz_{n-1}) + s(-z_{n-1} + f(X) \\ & - \hat{f}(X) + \widetilde{b}u - \rho s - \lambda \mathrm{sign}(s) + d(t)) + H \end{aligned} \tag{38}$$

Because (38) contains the approximation error of the function being estimated, bringing expression (33) into (38), $\dot{V}$ can be further derived as

$$\begin{aligned}\dot{V} = \; & -\sum_{i=1}^{n-1} k_i z_i^2 - c z_{n-1}^2 + \widetilde{b} s u + \widetilde{W}^T \hat{\Phi}_2 s + \hat{W}^T \Phi_{2B_1} \widetilde{B}_1 s \\ & + \hat{W}^T \Phi_{2C_1} \widetilde{C}_1 s + \hat{W}^T \Phi_{2W_r} \widetilde{W}_r s + \hat{W}^T \Phi_{2B_2} \widetilde{B}_2 s \\ & + \hat{W}^T \Phi_{2C_2} \widetilde{C}_2 s + \hat{W}^T \Phi_{2W_{\mathrm{ro}}} \widetilde{W}_{ro} s - \rho s^2 - \lambda |s| \\ & + s(\Delta_o + d(t)) + H\end{aligned} \tag{39}$$

The following adaptive laws of the DHLRNN are designed:

Defining $\widetilde{W}^T \hat{\Phi}_2 s + \frac{1}{\eta_1} \widetilde{W}^T \dot{\widetilde{W}} = 0$, it can be obtained that

$$\dot{\widetilde{W}} = -\eta_1 s \hat{\Phi}_2 \tag{40}$$

Defining $\hat{W}^T \Phi_{2B_1} \widetilde{B}_1 s + \frac{1}{\eta_2} \dot{\widetilde{B}}_1^T \widetilde{B}_1 = 0$, it can be obtained that

$$\dot{\widetilde{B}}_1^T = -\eta_2 s \hat{W}^T \Phi_{2B_1} \tag{41}$$

Defining $\hat{W}^T \Phi_{2C_1} \widetilde{C}_1 s + \frac{1}{\eta_3} \dot{\widetilde{C}}_1^T \widetilde{C}_1 = 0$, it can be obtained that

$$\dot{\widetilde{C}}_1^T = -\eta_3 s \hat{W}^T \Phi_{2C_1} \tag{42}$$

Defining $\hat{W}^T \Phi_{2W_r} \widetilde{W}_r s + \frac{1}{\eta_4} \dot{\widetilde{W}}_r^T \widetilde{W}_r = 0$, it can be obtained that

$$\dot{\widetilde{W}}_r^T = -\eta_4 s \hat{W}^T \Phi_{2W_r} \tag{43}$$

Defining $\hat{W}^T \Phi_{2B_2} \widetilde{B}_2 s + \frac{1}{\eta_5} \dot{\widetilde{B}}_2^T \widetilde{B}_2 = 0$, it can be obtained that

$$\dot{\widetilde{B}}_2^T = -\eta_5 s \hat{W}^T \Phi_{2B_2} \tag{44}$$

Defining $\hat{W}^T \Phi_{2C_2} \widetilde{C}_2 s + \frac{1}{\eta_6} \dot{\widetilde{C}}_2^T \widetilde{C}_2 = 0$, it can be obtained that

$$\dot{\widetilde{C}}_2^T = -\eta_6 s \hat{W}^T \Phi_{2C_2} \tag{45}$$

Defining $\hat{W}^T \Phi_{2W_{ro}} \widetilde{W}_{ro} s + \frac{1}{\eta_7} \dot{\widetilde{W}}_{ro}^T \widetilde{W}_{ro} = 0$, it can be obtained that

$$\dot{\widetilde{W}}_{ro}^T = -\eta_7 s \hat{W}^T \Phi_{2W_{ro}} \tag{46}$$

The parameter adaptive law of the control coefficient is designed as follows, which utilizes the calculation form of the adaptive projection algorithm

$$\dot{\hat{b}} = \mathrm{Proj}_{\hat{b}}(\eta_8 s u) \tag{47}$$

Remark 4. *The adaptive projection algorithm [20] can be defined as follows:*

$$\mathrm{Proj}_{\hat{b}}(\cdot) = \begin{cases} 0 & \hat{b} \geq b_l \text{ and } \cdot > 0 \\ 0 & \hat{b} \leq b_o \text{ and } \cdot < 0 \\ \cdot & \text{otherwise} \end{cases} \tag{48}$$

When $\hat{b}$ exceeds the maximum b_l and continues to increase, then $\dot{\hat{b}} = 0$, which means that $\hat{b}$ will remain unchanged. When $\hat{b}$ is less than the minimum b_o and continues to decrease, $\hat{b}$ will remain unchanged. In other cases, the adaptive law acts normally. To sum up, this algorithm can ensure the boundedness of the estimated term and avoid the sudden variation in $\hat{b}$ with different disturbances so that the control signal of the system can achieve stable control performance.

Substituting the above adaptive laws (40)–(47) into (39), $\dot{V}$ is simplified as

$$\dot{V} \leq -\sum_{i=1}^{n-1} k_i z_i^2 - c z_{n-1}^2 - \rho s^2 - \lambda |s| + s(\Delta_o + d(t)) \tag{49}$$

Because $|d(t)| \leq D$ and $|\Delta_o| \leq \overline{\Delta}_d$, then Equation (49) can be further expressed as

$$\dot{V} \leq -\sum_{i=1}^{n-1} k_i z_i^2 - c z_{n-1}^2 - \rho s^2 - \lambda |s| + s(D + \overline{\Delta}_d) \tag{50}$$

By selecting the switching term gain, as long as λ satisfies the condition of $\lambda > D + \overline{\Delta}_d$, the following result can be concluded:

$$\begin{aligned} \dot{V} &\leq -\sum_{i=1}^{n-1} k_i z_i^2 - c z_{n-1}^2 - \rho s^2 - (\lambda - D - \overline{\Delta}_d)|s| \\ &\leq -\sum_{i=1}^{n-1} k_i z_i^2 - c z_{n-1}^2 - \rho s^2 \\ &\leq 0 \end{aligned} \tag{51}$$

Because $\dot{V} \leq 0$ guarantees that $\dot{V}$ is semi$-$negative definite, according to the LaSalle invariance principle, when $t \to \infty$, $z_i = 0 (i = 1, 2, \cdots, n)$ and $s = 0$.

Meanwhile, the finite$-$time convergence of tracking error E is illustrated in Remark 5.

Remark 5. *According to Remark 1 and the expression of $p(t)$, when $t = 0$, $e^{(i)}(0) = p^{(i)}(0)$ $(i = 1, 2, \cdots, n-1)$. Therefore, it can be obtained that*

$$\begin{aligned} &z_1(0) = e(0) - p(0) = 0 \\ &z_2(0) = \dot{e}(0) - \dot{p}(0) - \alpha_1(0) = 0 \\ &z_3(0) = \ddot{e}(0) - \ddot{p}(0) - \alpha_2(0) = 0 \\ &\vdots \\ &z_n(0) = e^{(n-1)}(0) - p^{(n-1)}(0) - \alpha_{n-1}(0) = 0 \\ &s(0) = c z_{n-1}(0) + z_n(0) = 0 \end{aligned} \tag{52}$$

It can be seen from (52) *that all initial states of the system are already equal to zero, and it has been proven that $\lim_{t\to\infty} z_i = 0$ and $\lim_{t\to\infty} s = 0$, so the reaching condition of the BTSMC is eliminated. This means that the condition of $z_i = 0$ $(i = 1, 2, \cdots, n)$, $s = 0$ always holds; thus, it is deduced that $\alpha_i = 0$ $(i = 1, 2, \cdots, n-1)$ is always satisfied, and the global robustness of closed$-$loop system is guaranteed.*

Because the terminal function has ensured that $p(t) = 0$, $\dot{p}(t) = 0$, $\cdots$, $p^{(n-1)}(t) = 0$ for $t \geq T$, the tracking error E can be guaranteed to converge to zero in finite time.

Remark 6. *The unknown function $f(X)$ possesses a strong nonlinear characteristic; when faced with the inevitable system uncertainties and disturbances, its value will experience unexpected variation. Thus, the ideal control law (5) with the uncertainty term has a high−frequency fluctuation. In order to weaken the chattering phenomenon, the proposed controller utilizes the DHLRNN to estimate $f(X)$ for accurate feedforward compensation to observe the real−time variation in $f(X)$. The signum function $sign(\cdot)$ is adopted to compensate the approximation error. As long as an accurate approximation of the uncertainty term is obtained, the switching term gain is set to be small. Therefore, the discontinuous behavior of the controller can be effectively suppressed and the chattering is reduced.*

4. Simulation Study

In this section, a DC–DC buck converter model is built to verify the effectiveness of the proposed control method (ABTSMC−DHLRNN). The basic circuit framework of the model is shown in Figure 4, which comprises a load resistance R_0, a LC filter, a diode D, a PWM gate drive−controlled switch (insulated gate bipolar transistor) Q, and DC voltage V_{in}. The controlled switch ON and OFF cases are depicted with dashed lines 1 and 2, respectively.

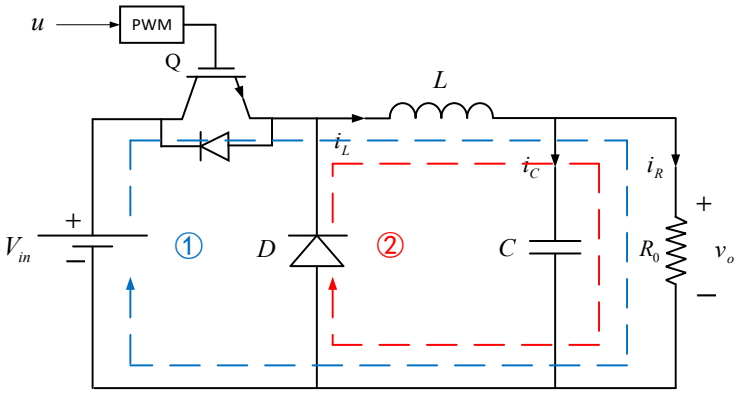

Figure 4. Circuit diagram of DC–DC buck converter (ON case: Line 1, OFF case: Line 2).

The Kirchhoff law and state space method are utilized here to analyze the circuit model. The dynamic model can be built along the following steps, where v_o and i_L denote output voltage and inductor current, respectively.

When controlled switch Q is turned on, v_o and i_L satisfy

$$\begin{cases} C\dfrac{dv_o}{dt} = i_L - \frac{v_o}{R_0} \\ L\dfrac{di_L}{dt} = V_{in} - v_o \end{cases} \tag{53}$$

When controlled switch Q is turned off, v_o and i_L satisfy

$$\begin{cases} C\dfrac{dv_o}{dt} = i_L - \frac{v_o}{R_0} \\ L\dfrac{di_L}{dt} = -v_o \end{cases} \tag{54}$$

Therefore, the dynamic model of the DC–DC buck converter can be written as

$$\begin{cases} \dfrac{di_L}{dt} = -\frac{1}{L}v_o + \frac{V_{in}}{L}u \\ \dfrac{dv_o}{dt} = \frac{1}{C}i_L - \frac{1}{R_0C}v_o \end{cases} \tag{55}$$

Then, the following second−order state equation is designed

$$\begin{cases} \dot{x}_1 = x_2 \\ \dot{x}_2 = f(x) + bu + d(t) \end{cases} \tag{56}$$

where $x_1 = v_o$ and $x_2 = \dot{v}_o$ represent state variables, $f(x) = -\frac{x_1}{LC} - \frac{x_2}{R_0 C}$, and $b = \frac{V_{in}}{LC}$.

Based on the design in Section 3, the control law (34) is applied to the simulation model.

The reference voltage is denoted as v_{ref}. The control objective of the buck converter is to design a control law, allowing the output voltage to quickly track the reference voltage trajectory. According to the state equation of the buck converter system, the ABTSMC with the DHLRNN is designed as

$$\begin{aligned} u = \quad & \tfrac{1}{\hat{b}}(-c(-k_1 z_1 + z_2) - z_1 - \hat{f}(x) \\ & + \ddot{v}_{ref} + \ddot{p} - k_1 \dot{z}_1 - \rho s - \lambda \mathrm{sgn}(s)) \end{aligned} \tag{57}$$

The nominal parameter values of the main circuit are summarized in Table 1. The switching frequency for IGBT is chosen as 10 kHz and the simulation sampling period is chosen as 10 µs.

Table 1. Model nominal parameters.

Description	Parameter	Value	Units
Input voltage	V_{in}	25	V
Reference voltage	v_{ref}	12	V
Inductor	L	6	mH
Capacitor	C	2200	µF
Load resistance	R_0	30	Ω
Switching frequency	f_{sw}	10	kHz
Sampling period	T_s	10	µs

To illustrate the superiority of the proposed control method, the ABTSMC control method without neural network approximation (ABTSMC) and BSMC based on the RBFNN (BSMC−RBFNN) are investigated here for comparison. The above controllers are simulated on a digital simulation platform using Matlab/Simulink software.

For fair comparison, the three control strategies are carried out under identical conditions to the simulation study, and the selection of the sliding mode gain is the same. The parameters of the above controllers are selected as listed in Table 2.

Table 2. Controller parameters.

Controllers	Parameters and Values
ABTSMC	$c = 4000$, $k_1 = 2 \times 10^5$, $\rho = 2000$, $\lambda = 1200$, $T = 0.01$
BSMC−RBFNN	$c = 4000$, $k_1 = 2 \times 10^5$, $\rho = 100$, $\lambda = 120$
ABTSMC−DHLRNN	$c = 4000$, $k_1 = 2 \times 10^5$, $\rho = 2000$, $\lambda = 1200$, $T = 0.01$

Remark 7. *The switching term gain existing in SMC affects the steady−state performance of the system. Due to the discontinuity of the signum function, too large a switching gain often brings the system chattering problem. Therefore, in order to highlight the neural network approximation, the switching gain is set to be small. The relevant sliding gain is set to be large for obtaining fast convergence. Moreover, with regard to the learning rates of the neural network, each parameter can be observed according to the response curve; thus, we can judge whether these parameters converge. Among them, output weight determines the output signal amplitude of the neural network; in order to cope with the high amplitude of the nonlinear function, the learning rate of the weight is set larger than the other parameters. When all the learning rates are set to the appropriate order of magnitude,*

the output signal can roughly track the reference trajectory. Then, they can be fine−tuned until the control objective is achieved.

To compare the performance of the above controllers under different uncertainties and disturbances, the buck converter is subjected to the following four situations: (1) start−up phase analysis, (2) load resistance variations, (3) reference voltage variations, and (4) input voltage variations.

In addition, the structure of the DHLRNN is selected as 2−4−3−1, and the learning rates in (40)–(47) are $\eta_1 = 2.6 \times 10^5$, $\eta_2 = 0.02$, $\eta_3 = 0.13$, $\eta_4 = 0.1$, $\eta_5 = 0.01$, $\eta_6 = 2 \times 10^{-5}$, $\eta_7 = 1 \times 10^{-10}$, and $\eta_8 = 16000$.

4.1. Start−Up Phase Analysis

The reference voltage is set to 12 V, and the load resistance remains unchanged at 30 Ω. The response curves obtained for the output voltage and inductor current are shown in Figure 5a,b, respectively. As shown in Figure 5a, due to the low compensation accuracy of the RBFNN, a satisfactory dynamic response is difficult to obtain. The BSMC−RBFNN method produces a larger output voltage overshoot during the start−up phase. Furthermore, due to the lack of terminal function, the tracking error will not converge in finite time. Therefore, the corresponding startup time is longer than those of other control strategies, which takes about 260 ms. Although the ABTSMC method can reduce the convergence time via introducing the terminal function, the problem of large output voltage overshoot also exists due to the lack of an estimation item of the nonlinear function in the controller.

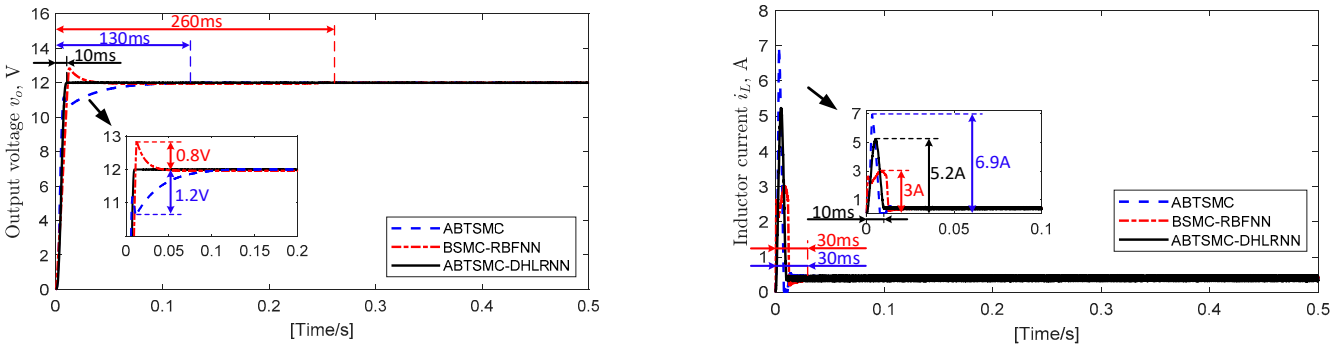

(**a**) (**b**)

Figure 5. Response curves of start−up phase. (**a**) Output voltage v_o, V. (**b**) Inductor current i_L, A.

On the contrary, the proposed control method tracks the reference voltage in 10 ms without overshoot. The behavior of inductor current as shown in Figure 5b also further illustrates the superiority of the proposed control method.

4.2. Load Resistance Variations

To verify the robustness of the above controllers toward load uncertainty, the reference voltage remains unchanged at 12 V, and the load resistance is changed from 30 Ω to 20 Ω at $t = 2s$. The load resistance variations are along the following settings:

$$R = \begin{cases} 30\ \Omega\ (= R_0), & t \in [0, 2) \\ 20\ \Omega\ (= \frac{2}{3} R_0), & t \in [2, 5] \end{cases} \tag{58}$$

The responses of v_o and i_L under such a variation are depicted in Figure 6a,b. It can be seen from Figure 6a that the proposed control method ensures faster settling time, with only a slight drop in output voltage waveform around the desired trajectory. The main reason is that the DHLRNN has accurately compensated the model uncertainty owing to load variations, whereas the ABTSMC method yields about a 0.02 V voltage drop due to

the inability to eliminate the undesirable impact of the external disturbances. Although the BSMC−RBFNN method produces a lower voltage drop during the load during the occurrence of load variations, the RBFNN takes a longer time to tune neural network parameters. As a result, it takes 50 ms to stabilize the output voltage and there exists an adverse overshoot, which may damage the performance of the buck converter.

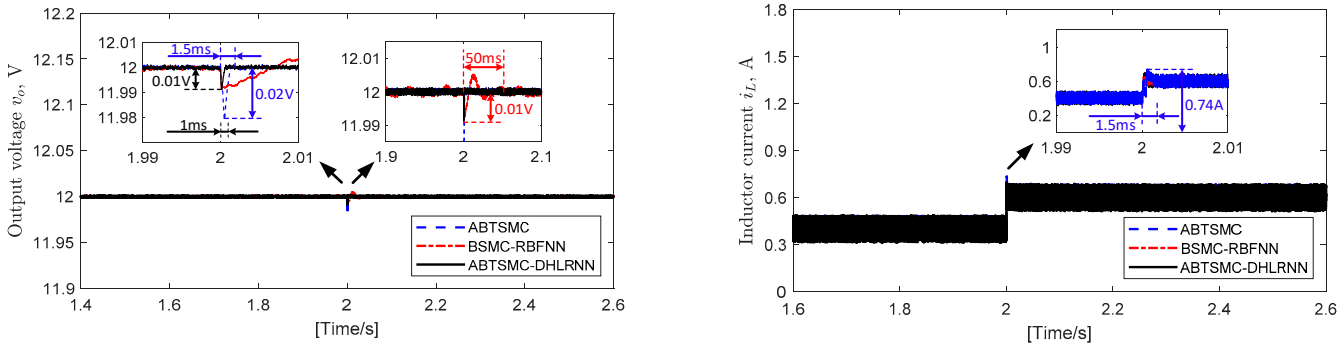

(**a**) (**b**)

Figure 6. Response curves with load resistance variations. (**a**) Output voltage v_o, V. (**b**) Inductor current i_L, A.

4.3. Reference Voltage Variations

The tracking performance of the above controllers is evaluated by changing the reference voltage from 12 V to 15 V at $t = 2$ s, and the load resistance remains unchanged at 30 Ω. The reference voltage variations are along the following settings:

$$v_{ref} = \begin{cases} 12 \text{ V}, & t \in [0, 2) \\ 15 \text{ V}, & t \in [2, 5] \end{cases} \tag{59}$$

The performance of the above controllers during the reference variations can be found in Figure 7a,b. Figure 7a illustrates that the ABTSMC and the BSMC−RBFNN methods are found to track the new reference trajectory in 600 ms and 180 ms, respectively. Compared with the neural network control method, the ABTSMC method fails to obtain satisfactory dynamic performance and reveals a slower response in rejecting reference value uncertainty, while the proposed control method successfully tracks the new reference voltage in 10 ms without an obvious voltage rise. Moreover, the corresponding inductor current as plotted in Figure 7b also achieves a faster response and smaller peak current under the proposed method. Hence, because of the combination of the DHLRNN and adaptive algorithm, the proposed control method has superior tracking performance.

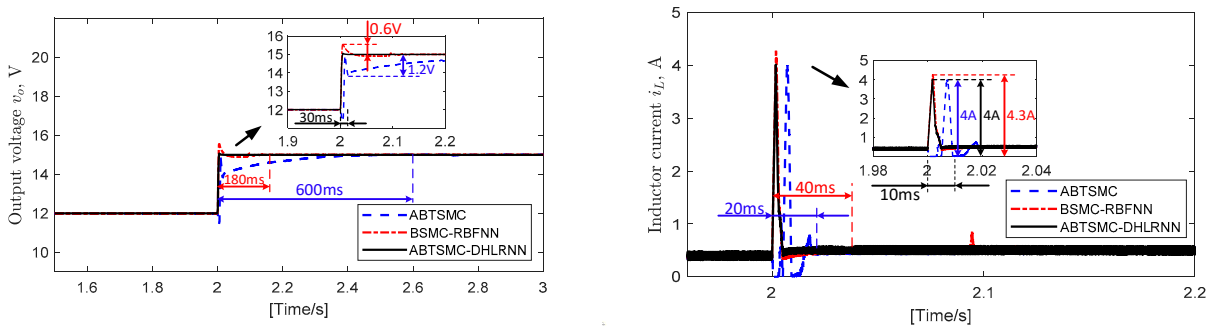

(**a**) (**b**)

Figure 7. Response curves with reference voltage variations. (**a**) Output voltage v_o, V. (**b**) Inductor current i_L, A.

4.4. Input Voltage Variations

Due to the long−term operation of the power source and external disturbance influences, the input voltage is difficult to maintain at the nominal value in the practical converter system, and the input voltage will fluctuate around the nominal value. In order to further investigate the steady−state performance of the above controllers toward the input voltage variations, a sawtooth disturbance with a period of 300 ms and amplitude of 2 V is introduced to simulate the input voltage fluctuations. The reference voltage remains unchanged at 12 V, and the load resistance remains unchanged at 30 Ω. Figure 8 shows the actual input voltage waveform in the presence of sawtooth disturbance.

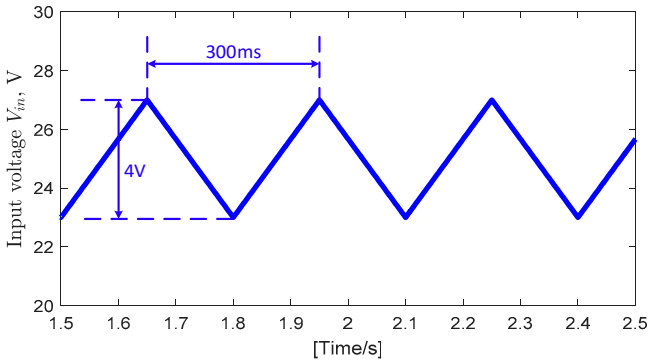

Figure 8. Waveform of real input voltage V_{in} with triangle disturbance.

Figure 9a,b show the responses of v_o and i_L. When dealing with the time−varying input voltage fluctuations, the BSMC−RBFNN method produces obvious sawtooth fluctuation. However, the output voltage waveforms of the ABTSMC and the proposed ABTSMC−DHLRNN methods are almost unchanged. The main reason is that both controllers adopt parameter adaptive laws to estimate the control coefficient, and a stable and accurate control law is obtained to remove the time−varying input effects. It can be seen that the proposed control method possesses better steady−state tracking performance and effective compensation for the input disturbances.

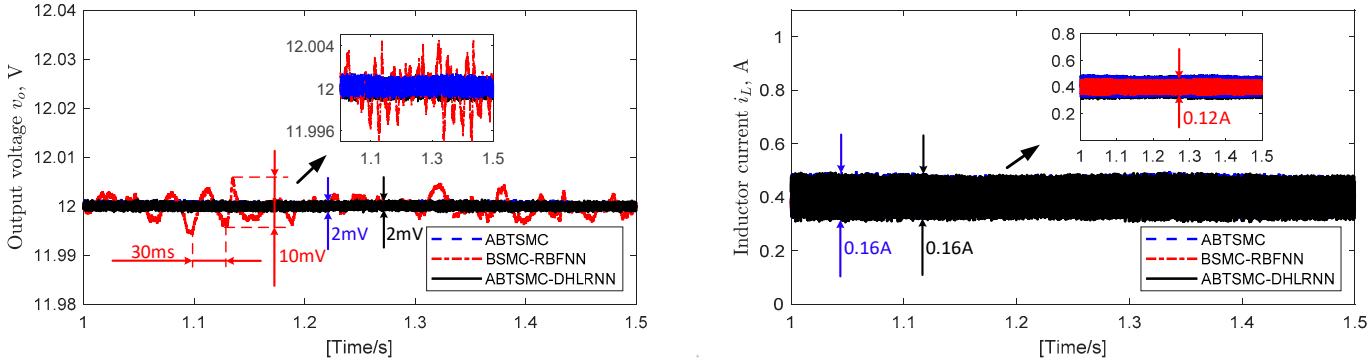

(**a**) (**b**)

Figure 9. Response curves with input voltage variations. (**a**) Output voltage v_o, V. (**b**) Inductor current i_L, A.

4.5. Comparison Analysis and Summary

In order to analyze and compare the performance of different controllers qualitatively, the performance indices are very useful, including maximum voltage rise/maximum voltage drop (MVR/MVD) and settling time (ST). They were widely used for comparison purposes in [44,45]. Table 3 lists the comparison results of performance indices. It is observed in Table 3 that the proposed control method ensures optimal indices in tracking

the reference voltage. Therefore, it can be confirmed that the proposed control method has better tracking accuracy and faster transient response speed, which improves the dynamic and steady−state performance of the converter system.

Table 3. Performance indices comparison in above situations.

Test	Controllers	Performance Indices	
		MVR/MVD (V)	**ST (ms)**
1	ABTSMC	−/1.2	−/260
	BSMC−RBFNN	0.8/−	130/−
	ABTSMC−DHLRNN	0/−	10/−
2	ABTSMC	−/0.02	−/1.5
	BSMC−RBFNN	−/0.01	−/50
	ABTSMC−DHLRNN	−/0.01	−/1
3	ABTSMC	−/1.2	−/600
	BSMC−RBFNN	0.6/−	180/−
	ABTSMC−DHLRNN	0.06/−	20/−
4	ABTSMC	0.001/0.001	−/−
	BSMC−RBFNN	0.006/0.004	−/−
	ABTSMC−DHLRNN	0.001/0.001	−/−

5. Conclusions

In this paper, an ABTSMC−DHLRNN method is designed for a class of SISO nonlinear system. To counteract and compensate for the system unknown uncertainty, the DHLRNN and parameter adaptive laws are utilized to estimate the nonlinear function and control coefficient, respectively. Based on the adaptive control theory, Lyapunov theorem, and finite−time convergence, the proposed ABTSMC−DHLRNN algorithm is designed. Although the nonlinear system operates under the presence of uncertainty and disturbances, the higher tracking accuracy and faster dynamic responses can be ensured. Furthermore, the proposed control method can guarantee the finite time convergence of the closed−loop system rigorously. The DHLRNN combines the merits of FNN, RNN, and MLNN, which obtains fewer neurons training and stronger approximation capacity. All the parameters of the network can adjust to optimal values through the adaptive learning algorithm, and the additional parameter adaptive laws adopt the expression form of the projection algorithm to ensure the boundedness of control coefficient estimates to obtain a stable control signal. Moreover, on the one hand, the backstepping design simplifies the control design steps; on the other hand, TSMC is introduced to guarantee that the tracking error can converge to zero in finite time. The proposed control method is applied to a second−order DC–DC buck converter system. The simulation result fully demonstrates its effectiveness and superiority in tracking the reference voltage. Considering other disturbed power systems, the proposed control method is designed for universal nonlinear systems, which can be directly applied without major modifications. The chattering problem still exists in SMC. Therefore, in future work, we will concentrate on how to further deal with the chattering problem of the control signal by using more advanced algorithms.

Author Contributions: Conceptualization, J.F.; methodology, X.G., W.F., and X.B.; writing—original draft preparation, X.G.; writing—review and editing, J.F. All authors have read and agreed to the published version of the manuscript.

Funding: This work is partially supported by the National Science Foundation of China under Grant No. 62273131.

Data Availability Statement: Not applicable.

Conflicts of Interest: The authors declare no conflict of interest.

Nomenclature

PID	Proportional−Integral−Derivative
SMC	Sliding mode control
TSMC	Terminal sliding mode control
BSMC	Backstepping sliding mode control
ABTSMC	Adaptive backstepping terminal sliding mode control
RBFNN	Radial basis function neural network
FNN	Fuzzy neural network
RNN	Recurrent neural network
DHLRNN	Double hidden recurrent neural network

References

1. Pan, Z.; Dong, F.; Zhao, J.; Wang, L.; Wang, H.; Feng, Y. Combined Resonant Controller and Two-Degree-of-Freedom PID Controller for PMSLM Current Harmonics Suppression. *IEEE Trans. Ind. Electron.* **2018**, *65*, 7558–7568. [CrossRef]
2. Hakan, U.; Irfan, O.; Ugur, Y.; Metin, K. Test Platform and Graphical User Interface Design for Vertical Take-Off and Landing Drones. *Rom. J. Inf. Sci. Technol. (ROMJIST)* **2022**, *25*, 350–367.
3. Lee, J.Y.; Jin, M.; Chang, P.H. Variable PID Gain Tuning Method Using Backstepping Control with Time-Delay Estimation and Nonlinear Damping. *IEEE Trans. Ind. Electron.* **2014**, *61*, 6975–6985. [CrossRef]
4. Meza, J.L.; Santibanez, V.; Soto, R.; Llama, M.A. Fuzzy Self-Tuning PID Semiglobal Regulator for Robot Manipulators. *IEEE Trans. Ind. Electron.* **2012**, *59*, 2709–2717. [CrossRef]
5. Precup, R.-E.; Preitl, S.; Rudas, I.J.; Tomescu, M.L.; Tar, J.K. Design and experiments for a class of fuzzy controlled servo systems. *IEEE/ASME Trans. Mechatron.* **2008**, *13*, 22–35. [CrossRef]
6. Incremona, G.P.; Rubagotti, M.; Ferrara, A. Sliding Mode Control of Constrained Nonlinear Systems. *IEEE Trans. Autom. Control* **2017**, *62*, 2965–2972. [CrossRef]
7. Zheng, X.; Yang, X. Command Filter and Universal Approximator Based Backstepping Control Design for Strict-Feedback Nonlinear Systems with Uncertainty. *IEEE Trans. Autom. Control* **2020**, *65*, 1310–1317. [CrossRef]
8. Cai, J.; Wen, C.; Su, H.; Liu, Z.; Xing, L. Adaptive Backstepping Control for a Class of Nonlinear Systems with Non-Triangular Structural Uncertainties. *IEEE Trans. Autom. Control* **2017**, *62*, 5220–5226. [CrossRef]
9. Lin, F.-J.; Huang, M.-S.; Chen, S.-G.; Hsu, C.-W.; Liang, C.-H. Adaptive Backstepping Control for Synchronous Reluctance Motor Based on Intelligent Current Angle Control. *IEEE Trans. Power Electron.* **2020**, *35*, 7465–7479. [CrossRef]
10. Ferrara, A.; Incremona, G.P. Design of an Integral Suboptimal Second-Order Sliding Mode Controller for the Robust Motion Control of Robot Manipulators. *IEEE Trans. Control. Syst. Technol.* **2015**, *23*, 2316–2325. [CrossRef]
11. Fei, J.; Feng, Z. Fractional-Order Finite-Time Super-Twisting Sliding Mode Control of Micro Gyroscope Based on Double-Loop Fuzzy Neural Network. *IEEE Trans. Syst. Man, Cybern. Syst.* **2021**, *51*, 7692–7706. [CrossRef]
12. Huang, S.; Wang, J.; Xiong, L.; Liu, J.; Li, P.; Wang, Z.; Yao, G. Fixed-Time Backstepping Fractional-Order Sliding Mode Excitation Control for Performance Improvement of Power System. *IEEE Trans. Circuits Syst. I Regul. Pap.* **2022**, *69*, 956–969. [CrossRef]
13. Zhang, J.; Sun, C.; Zhang, R.; Qian, C. Adaptive sliding mode control for re-entry attitude of near space hypersonic vehicle based on backstepping design. *IEEE/CAA J. Autom. Sin.* **2015**, *2*, 94–101.
14. Chen, F.; Jiang, R.; Zhang, K.; Jiang, B.; Tao, G. Robust Backstepping Sliding Mode Control and Observer-Based Fault Estimation for a Quadrotor UAV. *IEEE Trans. Ind. Electron.* **2016**, *63*, 5044–5056. [CrossRef]
15. Alipour, M.; Zarei, J.; Razavi-Far, R.; Saif, M.; Mijatovic, N.; Dragicevic, T. Observer-Based Backstepping Sliding Mode Control Design for Microgrids Feeding a Constant Power Load. *IEEE Trans. Ind. Electron.* **2023**, *70*, 465–473. [CrossRef]
16. Yu, X.; Man, Z. Fast terminal sliding-mode control design for nonlinear dynamical systems. *IEEE Tran. Circuits Syst. I Fundam. Theory Appl.* **2002**, *49*, 261–264.
17. Yao, X.; Park, J.H.; Dong, H.; Guo, L.; Lin, X. Robust Adaptive Nonsingular Terminal Sliding Mode Control for Automatic Train Operation. *IEEE Trans. Syst. Man Cybern. Syst.* **2019**, *49*, 2406–2415. [CrossRef]
18. Wang, H.; Zhang, Q.; Sun, Z.; Tang, X.; Chen, I.-M. Continuous Terminal Sliding-Mode Control for FJR Subject to Matched/Mismatched Disturbances. *IEEE Trans. Cybern.* **2022**, *52*, 10479–10489. [CrossRef]
19. Xu, B.; Zhang, L.; Ji, W. Improved Non-Singular Fast Terminal Sliding Mode Control with Disturbance Observer for PMSM Drives. *IEEE Trans. Transp. Electrif.* **2021**, *7*, 2753–2762. [CrossRef]
20. Oucheriah, S.; Guo, L. PWM-Based Adaptive Sliding-Mode Control for Boost DC–DC Converters. *IEEE Trans. Ind. Electron.* **2013**, *60*, 3291–3294. [CrossRef]
21. Chen, L.; Liu, M.; Huang, X.; Fu, S.; Qiu, J. Adaptive Fuzzy Sliding Mode Control for Network-Based Nonlinear Systems with Actuator Failures. *IEEE Trans. Fuzzy Syst.* **2018**, *26*, 1311–1323. [CrossRef]
22. Xu, L.; Yao, B. Adaptive robust control of mechanical systems with non-linear dynamic friction compensation. *Int. J. Control.* **2008**, *81*, 167–176. [CrossRef]
23. Zamfirache, I.A.; Precup, R.-E.; Roman, R.-C.; Petriu, E.M. Reinforcement Learning-based control using Q-learning and gravitational search algorithm with experimental validation on a nonlinear servo system. *Inf. Sci.* **2022**, *583*, 99–120. [CrossRef]

24. Yahui, L.; Sheng, Q.; Xianyi, Z.; Kaynak, O. Robust and adaptive backstepping control for nonlinear systems using RBF neural networks. *IEEE Tran. Neural Netw.* **2004**, *15*, 693–701.
25. Lian, J.; Lee, Y.; Sudhoff, S.D.; Zak, S.H. Self-Organizing Radial Basis Function Network for Real-Time Approximation of Continuous-Time Dynamical Systems. *IEEE Trans. Neural Netw.* **2008**, *19*, 460–474. [CrossRef]
26. Fei, J.; Chen, Y.; Liu, L.; Fang, Y. Fuzzy Multiple Hidden Layer Recurrent Neural Control of Nonlinear System Using Terminal Sliding-Mode Controller. *IEEE Trans. Cybern.* **2022**, *52*, 9519–9534. [CrossRef]
27. Fei, J.; Wang, H.; Fang, Y. Novel Neural Network Fractional-order Sliding-Mode Control with Application to Active Power Filter. *IEEE Trans. Syst. Man Cybern. Syst.* **2022**, *52*, 3508–3518. [CrossRef]
28. El-Sousy, F.; Amin, M.; Mohammed, O. Robust Optimal Control of High-Speed Permanent-Magnet Synchronous Motor Drives via Self-Constructing Fuzzy Wavelet Neural Network. *IEEE Tran. Ind. Appl.* **2021**, *57*, 999–1013. [CrossRef]
29. Fei, J.; Wang, Z.; Fang, Y. Self-Evolving Chebyshev Fuzzy Neural Fractional-Order Sliding Mode Control for Active Power Filter. *IEEE Trans. Ind. Inform.* **2022**. [CrossRef]
30. Lin, F.-J.; Hung, Y.-C.; Tsai, M.-T. Fault-Tolerant Control for Six-Phase PMSM Drive System via Intelligent Complementary Sliding-Mode Control Using TSKFNN-AMF. *IEEE Trans. Ind. Electron.* **2013**, *60*, 5747–5762. [CrossRef]
31. Han, H.-G.; Zhang, L.; Hou, Y.; Qiao, J.-F. Nonlinear Model Predictive Control Based on a Self-Organizing Recurrent Neural Network. *IEEE Trans. Neural Netw. Learn. Syst.* **2016**, *27*, 402–415. [CrossRef]
32. Fei, J.; Lu, C. Adaptive Sliding Mode Control of Dynamic Systems Using Double Loop Recurrent Neural Network Structure. *IEEE Trans. Neural Netw. Learn. Syst.* **2018**, *29*, 1275–1286. [CrossRef]
33. El-Sousy, F.; Abuhasel, K. Adaptive Nonlinear Disturbance Observer Using a Double-Loop Self-Organizing Recurrent Wavelet Neural Network for a Two-Axis Motion Control System. *IEEE Tran. Ind. Appl.* **2018**, *54*, 764–786. [CrossRef]
34. Lee, H.; Jung, M.; Tani, J. Recognition of Visually Perceived Compositional Human Actions by Multiple Spatio-Temporal Scales Recurrent Neural Networks. *IEEE Trans. Cogn. Dev. Syst.* **2018**, *10*, 1058–1069. [CrossRef]
35. Chen, H.; Wu, C.; Du, B.; Zhang, L.; Wang, L. Change Detection in Multisource VHR Images via Deep Siamese Convolutional Multiple-Layers Recurrent Neural Network. *IEEE Trans. Geosci. Remote Sens.* **2020**, *58*, 2848–2864. [CrossRef]
36. Makondo, W.; Nallanthighal, R.; Mapanga, I.; Kadebu, P. Exploratory test oracle using multi-layer perceptron neural network. In Proceedings of the 2016 International Conference on Advances in Computing, Communications and Informatics (ICACCI), Jaipur, India, 21–24 September 2016; pp. 1166–1171.
37. Xu, B.; Zhang, R.; Li, S.; He, W.; Shi, Z. Composite Neural Learning-Based Nonsingular Terminal Sliding Mode Control of MEMS Gyroscopes. *IEEE Trans. Neural Netw. Learn. Syst.* **2020**, *31*, 1375–1386. [CrossRef]
38. Fei, J.; Chen, Y. Fuzzy Double Hidden Layer Recurrent Neural Terminal Sliding Mode Control of Single-Phase Active Power Filter. *IEEE Trans. Fuzzy Syst.* **2021**, *29*, 3067–3081. [CrossRef]
39. Li, Y.; Zhang, J.; Liu, W.; Tong, S. Observer-based adaptive optimized control for stochastic nonlinear systems with input and state constraints. *IEEE Trans. Neural Netw. Learn. Syst.* **2021**, *33*, 7791–7805. [CrossRef]
40. Wang, Z.; Fei, J. Fractional-Order Terminal Sliding-Mode Control Using Self-Evolving Recurrent Chebyshev Fuzzy Neural Network for MEMS Gyroscope. *IEEE Trans. Fuzzy Syst.* **2022**, *30*, 2747–2758. [CrossRef]
41. Hua, M.; Zheng, D.; Deng, F. H∞ filtering for nonhomogeneous Markovian jump repeated scalar nonlinear systems with multiplicative noises and partially mode-dependent characterization. *IEEE Trans. Syst. Man Cybern. Syst.* **2021**, *51*, 3180–3192. [CrossRef]
42. Fei, J.; Chen, Y. Dynamic Terminal Sliding-Mode Control for Single-Phase Active Power Filter Using New Feedback Recurrent Neural Network. *IEEE Trans. Power Electron.* **2020**, *35*, 9904–9922. [CrossRef]
43. Fei, J.; Wang, Z.; Pan, Q. Self-Constructing Fuzzy Neural Fractional-Order Sliding Mode Control of Active Power Filter. *IEEE Trans. Neural Netw. Learn. Syst.* **2022**, 1–12. [CrossRef]
44. Babes, B.; Mekhilef, S.; Boutaghane, A.; Rahmani, L. Fuzzy Approximation-Based Fractional-Order Nonsingular Terminal Sliding Mode Controller for DC–DC Buck Converters. *IEEE Trans. Power Electron.* **2022**, *37*, 2749–2760. [CrossRef]
45. Lin, X.; Liu, J.; Liu, F.; Liu, Z.; Gao, Y.; Sun, G. Fractional-Order Sliding Mode Approach of Buck Converters with Mismatched Disturbances. *IEEE Trans. Circuits Syst. I Regul. Pap.* **2021**, *68*, 3890–3900. [CrossRef]